NOVA SCHOOL OF SCIENCE & TECHNOLOGY

DEPARTAMENT OF MATERIALS SCIENCE

BEATRIZ FIDALGO DA COSTA DEITADO

BSc in Micro and Nanotechnology Engineering

GREEN SYNTHESIS OF ZNO NANOSTRUCTURES

MASTER IN MICRO AND NANOTECHNOLOGY ENGINEERING

NOVA University Lisbon

September, 2023

DEPARTAMENT OF
MATERIALS SCIENCE

GREEN SYNTHESIS OF ZNO NANOSTRUCTURES

Beatriz Fidalgo da Costa Deitado

BSc in Micro and Nanotechnology Engineering

Adviser: Drª. Ana Pimentel
Principal Researcher, Cenimat/I3N, NOVA University Lisbon

Co-advisers: Msc. Alexandra Golçalves
Researcher, Cenimat/I3N, NOVA University Lisbon

Examination Committee:

Chair: Dr. Rodrigo Ferrão de Paiva Martins,
Full Professor, FCT-NOVA

Rapporteurs: Drª. Daniela da Silva Nunes Gomes,
Assistant Professor, FCT-NOVA

Adviser: Drª. Ana Cláudia Madeira Botas Gomes Pimentel,
Principal Researcher, Cenimat/I3N, FCT-NOVA

MASTER IN MICRO AND NANOTECHNOLOGY ENGINEERING

NOVA University Lisbon
September, 2023

Green synthesis of ZnO nanostructures

Para os meus pais.

ACKNOWLEDGMENTS

I extend my sincere appreciation to my academic advisors, Ana Pimentel, and Alexandra Gonçalves, for their invaluable guidance, support, and mentorship throughout this research journey. Your expertise and dedication have been instrumental in shaping this work. I am also grateful to Vanessa Pereira and her wonderful team in the Membrane Processes Lab at iBET, and Maria Leonor Matias for their insightful contributions and constructive feedback during this study. Your input greatly enriched the quality of this research.

I would like to acknowledge the Universidade NOVA de Lisboa for providing a conducive academic environment and access to resources that facilitated my research. The Materials Department, i3N/CEN-IMAT, CEMOP, iBET, ITQB, and NOVA School of Science and Technology have been integral to the successful completion of this project.

To my dear friends and colleagues, Carolina Pisica, Filipa Matos, Rita Simões, and Guilherme Gomes, your unwavering support, encouragement, and occasional study sessions made this academic journey not only bearable but enjoyable.

To my loving family and boyfriend, your patience, understanding, and belief in my abilities have been my pillars of strength. This achievement is as much yours as it is mine. Finally, to all those whose names may not appear here but whose contributions, no matter how small, have left an indelible mark on my life and this thesis, I extend my heartfelt gratitude.

This thesis would not have been possible without the collective support and encouragement I received from these individuals and institutions. Thank you all for being a part of this remarkable journey.

“O verdadeiro laboratório é a mente, onde são elaboradas as ideias.”
(Antero Quintal).

ABSTRACT

Zinc oxide (ZnO) is a wide direct band gap semiconductor with high exciton binding energy. Thus, it has superior photocatalytic performance, effectively in the photodegradation of organic pollutants. Nanostructures based on ZnO have many other applications such as antibacterial and antimicrobial. They can be synthesized by various methods, physical or chemical. Traditional approaches are costly and challenging to scale up while generating toxic chemicals.

This work uses natural extracts to synthesize more biocompatible ZnO nanostructures that are eco-friendly, safe, simple, cost-effective, and energy-saving. These include various types of acacias (*A. mearnsii* and *A. melanoxylon*) and pines (*P. nigra*, *P. sylvestris*, *P. pinea*, and *P. pinaster*), *Schoenoplectus lacustris*, and *Stryphnodendron*. A thorough examination was conducted on each plant and the respective nanostructures synthesized from them. X-ray diffraction (XRD) analysis confirmed the presence of ZnO in the samples, as well as the crystallinity index. Their structural and elemental characterization was carried out by scanning electron microscopy (SEM) coupled with energy-dispersive X-ray spectroscopy (EDS).

Plant-based ZnO nanostructures were successfully obtained by solvothermal microwave-assisted synthesis at 140ºC, 100W, for 20 minutes, using a high pH solvent, with zinc acetate as the precursor. The most favorable plant-based ZnO nanostructures were obtained from *A. mearnsii*, *P. sylvestris*, and *Stryphnodendron*. Due to its substantial opportunity to complement the literature, this work has been centered on the latter.

Afterward, optimal plant-based ZnO nanostructures were applied as photocatalyst agents and bacterial inactivators. The photocatalytic activity was evaluated under solar radiation, rhodamine B was the model-test contaminant indicator, and the best photocatalytic action was achieved with barbatimão-based ZnO, reaching 59% dye degradation, compared with the reference with just 13%. However, these nanostructures showed no significant antibacterial properties against *Escherichia coli*. It is necessary to conduct further tests in this area to understand their antibacterial potential.

Keywords: zinc oxide, nanostructures, green synthesis, natural extracts, photocatalysis, Barbatimão, *Stryphnodendron*, antibacterial.

RESUMO

O óxido de zinco (ZnO) é um semicondutor que apresenta um desempenho fotocatalítico superior, eficaz na fotodegradação de poluentes orgânicos. Nanoestruturas baseadas em ZnO têm muitas outras aplicações, tais como antibacterianas e antimicrobianas. Estas podem ser sintetizadas por vários métodos, mas as abordagens tradicionais são dispendiosas, difíceis de escalar, e ainda produzem químicos tóxicos.

Este trabalho utiliza extratos naturais para sintetizar nanoestruturas de ZnO mais biocompatíveis que sejam ecológicas, seguras, simples, economicamente eficientes e energicamente eficazes. Estes incluem vários tipos de acácias (*A. mearnsii* e *A. melanoxylon*) e pinheiros (*P. nigra*, *P. sylvestris*, *P. pinea* e *P. pinaster*), *Schoenoplectus lacustris* (bunho) e *Stryphnodendron* (barbatimão). Foi realizada uma análise detalhada de cada planta e das respetivas nanoestruturas sintetizadas a partir delas. A análise de difração de raios-X (XRD) confirmou a presença de ZnO nas amostras, enquanto a caracterização estrutural e elemental foi realizada por microscopia eletrónica de varrimento (SEM) acoplada à espectroscopia de raios-X por dispersão de energia (EDS).

As nanoestruturas de ZnO à base de plantas foram obtidas com sucesso por um síntese solvotermal assistida por micro-ondas a 140 °C, 100W, durante 20 minutos, usando àgua deionizada alcalina e acetato de zinco. As mais favoráveis foram obtidas a partir de extratos de casca de *A. mearnsii*, *P. sylvestris* e *Stryphnodendron*.

Esta última foi aplicada como agente fotocatalítico e inativador bacteriano, devido à considerável oportunidade de complementar a literatura neste tópico. A atividade fotocatalítica foi avaliada sob radiação solar, tendo a rodamina B sido o indicador de contaminante modelo de teste, atingindo uma degradação de 59% do corante, em comparação com apenas 13% da refernência. No entanto, estas nanoestruturas não demonstraram propriedades antibacterianas significativas contra a *Escherichia coli*. São necessários testes adicionais nesta área para compreender o seu potencial antibacteriano.

Palavas chave: óxido de zinco, nanoestruturas, síntese verde, extratos naturais, fotocatálise, Barbatimão, Stryphnodendron, antibacteriano.

CONTENTS

LIST OF FIGURES

LIST OF TABLES

ABBREVIATIONS

ZnO	Zinc Oxide.
NP	Nanoparticle.
MW	Microwave.
LED	Light Emitting Diode.
UV-Vis	Ultraviolet-Visible.
RhB	Rhodamine B.
SEM	Scanning Electron Microscopy.
EDS	Energy Dispersive X-ray Spectroscopy.
XRD	X-ray Diffraction.
DSC	Differential Scanning Calorimetry.
TG	Thermogravimetry.
LB	Luria-Bertani medium.
OD	Optical Density.
CFU	Colony Forming Unit.
CI	Crystallinity Index.

NOTATION

λ_{max}	The maximum wavelength.
r	The degradation rate of the reactant.
t	The illumination time.
K	The adsorption coefficient of the reactant.
k	The reaction rate constant.
C_0	The initial concentration of the reactant.
C	The concentration of the reactant corresponds to different time intervals.
A_0	The initial absorbance.
A	The absorbance at time intervals.

1

INTRODUCTION

Water pollution poses a severe threat to ecosystems and human health, particularly pollutants such as antibiotics, heavy metals, chlorophenols, dyes, and pesticides (1). Antibiotics are widely used in various industries, including the pharmaceutical sector (2,3), which results in their continuous release into the environment. This uncontrolled discharge of antibiotics contributes to antibiotic-resistant bacteria emergence and disrupts natural ecosystems.

Conventional procedures used for wastewater treatment result in incomplete removal of pollutants (4), time consumption, and high cost. These methods can be chemical (5), physicochemical (6), or biological, using techniques such as filtration (7), reverse osmosis (8), electrochemical treatment, distillation (9), ion exchange (10), and adsorption (11).

In recent years, the increasing concern about environmental pollution and the urgent need for effective water treatment methods have led to significant interest in the development of advanced nanomaterials. Zinc oxide (ZnO) nanostructures have emerged as promising candidates in the treatment of polluted water due to their unique properties.

Furthermore, ZnO nanostructures' antibacterial properties have garnered significant interest in their potential applications in clinical settings. As antibiotic-resistant bacteria become more prevalent, alternative antibacterial agents become more urgently needed. ZnO nanostructures possess inherent antimicrobial properties, making them a promising candidate for inactivating bacteria.

This study aims to explore ZnO nanostructure synthesis through an environmentally friendly and sustainable approach. By utilizing natural extracts, such as barbatimão bark extract, as reducing, capping, and stabilizing agents, the green synthesis method offers several advantages, including low toxicity, cost-effectiveness, and eco-friendliness, enhancing their potential for these applications.

1.1 ZnO nanostructures

With its high melting point (2248 K) and cohesive energy (1.89 eV), zinc oxide is the hardest II-VI metal compound, as well as one of the most piezoelectric semiconductors (12.2×10^{-12} C/N) (12). ZnO is also characterized by a wide direct bandgap (3.37 eV) and large excitation binding energy (60 meV) (13).

Working with nanostructures or nanoparticles (NPs) has its advantages when compared with the macro-size material, like conferring enhanced catalytic reactivity, thermal conductivity, non-linear optical performance, and chemical steadiness on account of its large surface area to volume ratio (14). As well as adjustable and morphological, photonic, and spintronic properties. Hence, ZnO NPs are among the top 3 most-produced nanomaterials. Most commonly, they are used in sunscreens, because their wide band gap allows them to transmit visible light while still effectively absorbing UV light (15).

1.2 Green synthesis methods

The synthesis of nanostructures can take a variety of approaches depending on whether it is performed from the top-down or the bottom-up perspective. In bottom-down manufacturing, nanomaterials are created from atoms or molecules, whereas in top-down manufacturing, bulk materials undergo milling and attrition to produce nano-scale products.

Traditional physical methods are expensive, require large equipment, and entail high temperatures and pressures during operation, which makes them unsuitable in many cases. Chemical versions involve the use of potentially hazardous chemicals that are not environmentally friendly and can be harmful to people and the environment (16).

So far, several chemical methods have been practiced, including chemical microemulsion, wet chemical, spray pyrolysis, electrodeposition, chemical, and direct precipitation, and microwave-assisted combustion (14), where no pollutant or combustible side product is produced. There can be also considered the physical methods of pulsed laser deposition and thermal evaporation. All are still in their infancy of development and still need improvement in the control of the size and shape of NPs obtained.

To meet the growing demand for environmentally friendly nanoparticles, new green methods are being explored to synthesize various metal nanoparticles using renewable resources. The advantages of green synthesis when compared with traditional methods of manufacturing include simplicity, safety, eco-friendliness, cost-effectiveness, biocompatibility, and scalability.

Natural extracts and nontoxic chemicals can be used to develop ZnO nanostructures. Literature reports the use of the plant, leaves, fruit, flower, and seed extracts, which act as reducing materials and stabilizing agents to establish the desired shape of the nanostructures.

Plant extracts achieve these desired effects because of their phenolic compounds, which have antioxidant properties and ensure the reduction process. Plants rely on flavonoids and other phenolic compounds in their leaf and flowering tissues, as well as woody parts such as stems and bark. This is for healthy growth and defense against infection or injury (17).

Additionally, they contain amino acids, proteins, and lipids that help stabilize growth and prevent the agglomeration of nanoparticles. Due to the presence of hydroxyl, carbonyl, and amine functional groups, these plant metabolites are reduced in size to the nanoscale when they react with metal ions (18,19). Thus, it is reported that the hydroxyl group from flavonoids is the cause of the reduction of metal ions in NPs (20).

1.2.1 Optimum conditions

To produce better ZnO nanostructures and achieve better results for their applications, several parameters were studied and optimized throughout this project.

Many factors influence the size, shape, orientation, and morphology, such as pH level, precursor concentration, doping, quenching effect, reaction (growth) time, reaction (growth) temperature, and calcination (annealing) temperature, which may all be regulated (21). In this work, the goal is to use a temperature inferior to 200 ºC, less than 30 minutes of synthesis, and power below 200 W.

Regarding pH, it has been studied the effect of several pH values on the characteristics of the green synthesis ZnO NPs quality and obtained the optimum pH value (22). According to Mahdi Ismail et al., 2023, the green synthesized ZnO NPs produced at pH 8 showed superior quality and a significant improvement compared to the ZnO NPs produced at lower pH values, therefore favoring high pH settings (alkaline) (22).

The precursor of choice is zinc acetate due to its various advantages over others and favorable results in the literature. Nanoparticles synthesized from zinc acetate were found to possess higher bioactivity than zinc nitrate, sulfate, and chloride, according to the work of Gatou et al., 2022. In summary, the data showed that the enhanced photocatalytic and biological activity of ZnO NPs derived from zinc acetate precursors might have been attributed to a reduction in crystalline size, increased surface area, and a hexagonal crystal structure (23).

1.2.2 Natural extracts

In recent years, there has been a growing recognition of the invaluable potential of harnessing natural extracts, particularly those derived from plants, in scientific research. The natural extracts tested in this project were from plants native to the Mediterranean and Eastern European regions. These plants include various types of acacias (A. *mearnsii* and *A. melanoxylon)* and pines (*P. nigra*, *P. sylvestris*, *P. pinea*, and *P. pinaster*), *Schoenoplectus lacustris*, and *Stryphnodendron*. The most promising results were from acacias and *Stryphnodendron*. The latter received the most attention since there aren't any publications on green nanostructure synthesis. This is an excellent opportunity to add to the literature on this topic. Based on this variety, the most widely described nanostructures in the literature are acacia-based, as shown in Table 10 (see annex A.1).

This approach not only offers eco-friendly and sustainable solutions but also taps into the entirety of the plant's resources, reducing waste and maximizing utility. Traditionally, various components of plants, such as bark, leaves, and needles, often went underutilized or were considered waste material. However, through innovative research endeavors like this one, we aim to unlock the latent value within these botanical resources, opening new avenues for green synthesis and environmental applications.

1.2.2.1 Barbatimão

Stryphnodendron Species, commonly known as "Barbatimão", is a native Brazilian tree, from the *Fabaceae Lindl.* Family was employed to synthesize ZnO nanostructures since it presents various advantages for this study.

Scientific studies have explored the Barbatimão ethnopharmacological uses of various treatments, including wound healing, anti-inflammatory measures, oral antimicrobial methods for genitourinary infections (specifically targeting gram-positive bacteria and *Candida* species), peripheral antinociception for pain relief, and addressing gastric ulcers (although toxicity was observed in some cases). Additionally, antioxidant effectiveness has been widely evaluated, but conclusive findings regarding anticancer activity have yet to be determined (24).

These medicinal properties can be attributed to phenolic compounds, especially tannins. Tannins are biodegradable, non-toxic, non-corrosive, and renewable. Plants with high tannin concentrations represent a major source of inspiration for drug development. Several studies (25) have indicated that hydrolyzable and condensed tannins can sustain antibacterial activity against a wide range of bacteria.

Due to its close relationship between therapeutic dose and toxicity, barbatimão is very toxic to many living species. It is generally considered safe for human use when used in moderation and following traditional practices.

The potential for diversified use of barbatimão bark can be a significant step towards species conservation, in addition to encouraging increased plantings, since obtaining the bark can be done by non-destructive methods, making this study and various others relevant to sustainability.

1.3 Photocatalytic activity

Degradation using photocatalytic processes is an advanced oxidation process that improves biodegradability and reduces the concentration of pollutants. By absorbing photons in visible, ultraviolet, and infrared wavelengths, pollutant molecules are oxidized and hydrolyzed. Light activates the photocatalytic material, causing the photo-responsive electron to migrate from the valence to the conduction band. As a result of photochemical reactions, electrons and holes produced by the photo process react with oxygen, water, and hydroxyl groups to produce reactive oxygen species, such as hydroxyl radicals and superoxide radical anions (26). By interacting with pollutant molecules, these radicals can partially or entirely degrade persistent pollutants. ZnO nanostructures photocatalytic mechanism can be understood from the scheme in Figure 1.

The most used photocatalysts have some limitations since they only show photocatalytic effect in the UV region, which is caused by the wide band gaps between the valence and conduction bands. Hence, these materials require higher energy light sources. However, the plant-based ZnO nanostructures will be evaluated in VIS region, since ZnO exhibits a high absorption capacity with a broad solar spectrum.

After synthesizing the most favorable nanostructures, their photocatalytic activity will be assessed by investigating the degradation efficiency of pollutants, under simulated sunlight conditions, thereby addressing energy and environmental concerns (27).

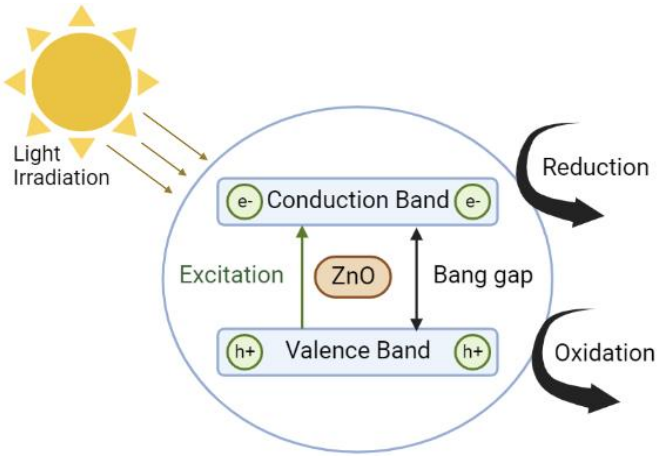

Figure 1. Illustration of photocatalytic mechanisms of ZnO nanostructures. Created in BioRender.com

1.4 Antibacterial activity

Antimicrobial resistance severely threatens public health worldwide, affecting several treatments' efficacy. These nanostructures have a high potential to be an antibacterial agent, both because of the medicinal properties of barbatimão, as mentioned before, as well as the inherited properties of ZnO NPs.
It has been suggested that ZnO nanoparticles might damage the cell membranes of bacteria. This would lead to the lysis of the internal contents of the cells and ultimately result in the cells' death (37). It should be noted that the antimicrobial action of ZnO nanostructures occurs in a manner that destroys cell integrity whilst forming reactive oxygen species (ROS) and releasing metal ions such as Zn(II) (38).
As referred to in Chapter 1.2.2, the plants' high tannin content enhances their antibacterial capacity. This may be attributed to the inhibition of extracellular microbial enzymes, deprivation of microbial growth substrates, or direct action on microbial metabolism through the inhibition of oxidative phosphorylation. Another option may involve iron deprivation (30).
Escherichia coli is a Gram-negative bacterium commonly used in teaching and research laboratories. It can also indicate possible sewage contamination because it is frequently found in human and animal feces. Therefore, due to the antibacterial and photocatalytic potential, the plant-based ZnO nanostructures, namely the optimized ones with barbatimão bark extract, were tested to inactivate *E.* coli, with and without LED irradiation.

2

MATERIALS AND METHODS

2.1 Natural extracts

Various plants native to the Mediterranean and Eastern European regions were tested for their ability to produce ZnO nanostructures. Namely, from the *Cyperaceae* Family: *Schoenoplectus lacustris*, from the *Pinaceae* Family: *Pinus pinea*, *pinaster*, *sylvestris*, and *nigra*, and from the *Fabaceae* Family: *Stryphnodendron* (Barbatimão), *Acacia mearnsii*, and *melanoxylon*. These extracts were either from bark, needles, or wood. All were provided by ISA (Instituto Superior de Agronomia) and were properly characterized for their phytochemicals.

The natural extracts were prepared by adding a varying quantity of extracts (from 0.1g to 1g) to 100 ml of solvent (deionized water). The mixture was boiled at 80 ºC for 1 hour with a 600 rpm stir. Then it was filtered with a paper filter and stored in the fridge for later use.

2.2 MW-assisted synthesis

The ZnO structures were synthesized by adding the precursor to the plant infusion that was previously prepared, following a standardized ratio of 1.375 g of zinc acetate dihydrate, ACS, 98.0-100.0% crystalline $Zn(OOCCH_3)_2 \cdot H_2O$ by Alfa Aesar (zinc precursor) per 100 mL of deionized water, with two different pH (6.8 and 9.1) (solvent).

Discover ® SP Microwave Synthesizer was employed to assist the reaction, taking 20 ml of mixture, for 20 minutes, with maximum pressure set to 280 psi, and power of 100W to test the different temperatures: 100, 140, and 180 ºC.

The resulting structures were cleaned by alternating deionized water and isopropanol, recurring to a Centrifuge Neya 8 and 16, set to 6000 rpm for 3 minutes each time at room temperature. Then, the supernatant was discarded, and the nanostructures were left to dry in open tubes in a fume hood for 3 days. A scheme of this procedure can be found in Figure 19 in annex A.1.

2.3 Characterization

The morphology of the nanostructures has been characterized by Scanning Electron Microscopy (SEM) using a a Hitachi Regulus 8220 Scanning Electron Microscope (Mito, Japan) equipped with an Oxford X-ray Energy Dispersive Spectrometer (EDS) detector. X-ray Diffraction (XRD) measurements have been carried out by an X-ray diffractometer by PANalytical X'Pert PRO MRD, from 15º to 70º (2θ),

with a scanning step size of 0.016º. Simultaneous thermal analyzer STA 449 F3 Jupiter was employed to study the natural extracts for its Differential Scanning Calorimetry (DSC) and Thermogravimetry (TG) features, in an air atmosphere until it reached 550 ºC with a heating rate of 10 K/min, and an aluminum (Al) crucible where, approximately, 14 mg of sample was placed.

2.4 Photocatalysis Experiments

A preliminary test was done to test the different plants used to synthesize ZnO nanostructures for their photocatalytic potential, considering dye degradation.

Firstly, a 30 ml aqueous suspension of Rhodamine B (RhB) dye from Sigma-Aldrich loaded with a photocatalyst, with an initial concentration of 10^{-5} M, was mixed with 25 mg of sample. The suspension was allowed to attain adsorption-desorption equilibrium in a dark atmosphere and stirred for 15 min. This time is typically higher, but with the various tests done, it was needed to shorten it. This is because the reactions between the powder and RhB happened very quickly.

Solar light exposure was conducted by using a WAVELABS LS-2 LED solar simulator (Germany) with AM 1.5 spectrum, at an intensity of 100 mW/cm^2. In some cases, these tests were also conducted in natural sunlight at peak hours with (a UV index of approximately 7).

Every sample was duplicated in the dark for control, as well as an individual test of the RhB solution alone. ZnO and the plant extract, individually, were used as references for our plant-based ZnO nanostructures.

The solution samples were withdrawn at 15 to 60-minute intervals and centrifuged at 10000 rpm for 1 minute at room temperature. The change in the absorbance at a maximum wavelength (λ_{max} = nm) of dye was monitored using a PerkinElmer double-beam LAMBDA 365+ UV/Vis Spectrometer (Waltham, MA, USA). The absorbance (A) was obtained from 400 to 700 nm.

2.5 *E. coli* inactivation by photocatalyst

E. coli colony was grown in LB (Luria-Bertani) medium following a standard protocol by Tuttle, Trahan, and Son, 2021 (28). Firstly, an isolated colony of *E. coli* was tipped with 300 mL of LB medium. The Erlenmeyer was incubated at 37 ºC ON. Control was made with LB medium and a sterile tip that was also incubated at 37 °C ON to check the sterility of the tips and the culture medium. Afterwards, an *E. coli* cell suspension was made with an optical density (OD) of approximately 0.4 which corresponds to ~ 10^7 CFU / mL. Calibration measurements on the radiometer were also taken so that the plant-based ZnO nanostructures could be tested on the bacterial cell suspension.

The photocatalysis tests included positive controls (bacteria without any treatment) and negative controls (bacteria treated under non-photocatalytic conditions), with a total of 20 minutes of exposure. Following the tests, the initial samples were diluted. Then, the dilutions were incubated on to the plates for later counting. These studies were conducted in iBET-ITQB NOVA (Instituto de Biologia Experimental e Tecnológica - Instituto de Tecnologia Química e Biológica António Xavier).

3

RESULTS AND DISCUSSION

3.1 Optimized Synthesis Parameters

3.1.1 Temperature study

Firstly, three ZnO reference samples (without natural extracts) were synthesized at different temperatures: 100, 140, and 180 ºC, to determine at which of these there was the formation of ZnO from the zinc acetate precursor. Remember that the goal is to use lower temperatures, preferably less than 200 ºC. XRD was used to provide the samples' chemical composition, structural characteristics, and physical properties.

Considering our references, we can observe that ZnO wasn't formed at 100 ºC, but it was possible to obtain it at 140 ºC. The peaks of ZnO reference synthesized at 140 ºC coincide with the stick pattern of ZnO 01-080-0074, as can be observed in Figure 2. Therefore, there isn’t the need to reach the higher temperature of 180 ºC that had been hypothesized.

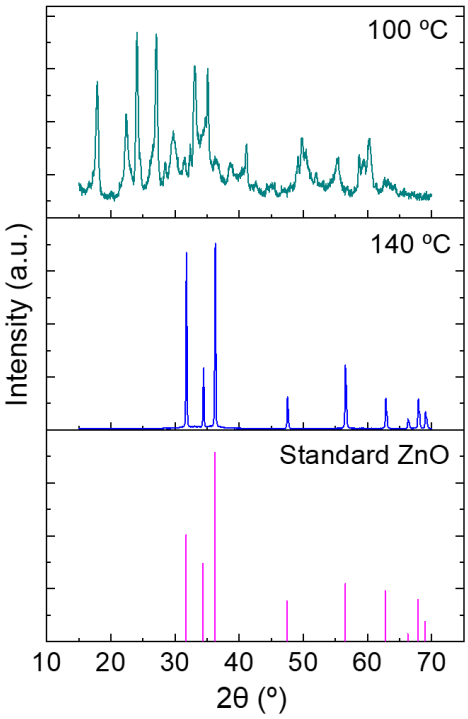

Figure 2. XRD patterns for standard ZnO and ZnO reference samples (without natural extracts) synthesized with zinc acetate at 100 and 140 °C, in a MW for 20 minutes.

The Crystallinity Index (CI), which is a quantitative indicator of crystallinity, was calculated after confirming the presence of ZnO in the reference samples at 140 ºC. It is the ratio of the crystalline peaks to the crystalline plus amorphous peaks, as can be seen in the equation (29):

$$CI = \frac{Area\ of\ all\ crystalline\ peaks}{Area\ of\ all\ crystalline\ and\ amorphous\ peaks} \quad (1)$$

From XRD Integration Method, using Origin software, it was possible to calculate a CI as high as 76% for the ZnO reference at 140 ºC.

3.1.1.1 Natural extracts

DSC allows studying at which temperature it begins to degrade. Combined with TG, this device measures mass changes and thermal effects over time and temperature. It is helpful for comparisons since it is known that zinc acetate decomposes at around 230 ºC, allowing us to better determine the working temperature for our plant-based ZnO nanostructures. This ensures that the nanostructure's size and shape aren´t affected by the integrity of the plant extract.

The first indication of mass loss in barbatimão bark extract, Figure 3, may imply the loss of water residual in natural extracts such as this one, so it isn't considered a degradation of the sample at that temperature. It is only the second mass change that is relevant. The natural extract begins to degrade at approximately 160 ºC, but not significantly until 200 ºC, which corroborates the temperature choice of 140 ºC.

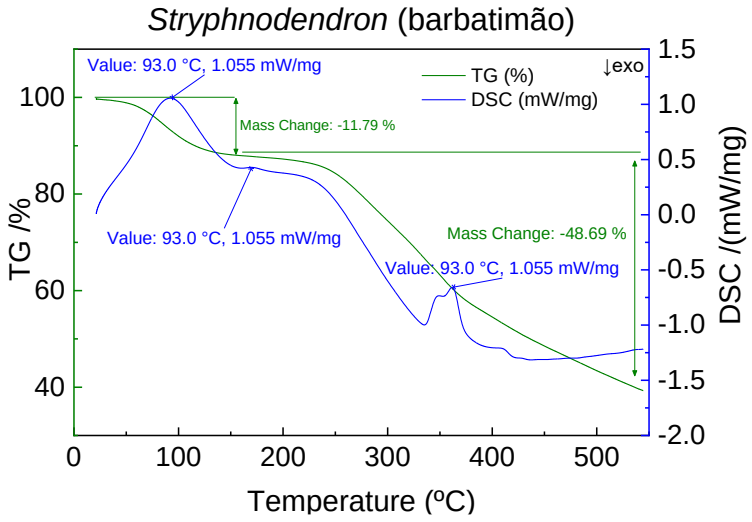

Figure 3. Barbatimão bark extracts simultaneous thermal analysis with DSC.

The other plant extracts used were also submitted to this study (see Figures 20 to 22 in annex A.2). A summary of this analysis can be found in Table 1. Even though acacias have a higher working temperature than their counterparts, the smallest temperature interval of all the natural extracts combined must be the one considered. Here, the highest minimum temperature and the lowest maximum temperature are 100 and 150 ºC, respectively. As a result, this is the working temperature interval that is common to

all plants, and thus, the optimum temperature for the synthesis of ZnO falls within this range, which indicates that 140 ºC is the perfect temperature to conduct this study.

Table 1. Working temperature intervals of plant extracts used, with DSC analysis.

Plant Extract	Working temperature interval (ºC)
Acacia mearnsii	[60, 210]
Acacia melanoxylon	[60, 190]
Stryphnodendron	[100, 160]
Schoenoplectus lacustris	[70, 150]
Pinus nigra	[70, 150]
Pinus sylvestris	[60, 180]
Pinus pinea	[80, 160]
Pinus pinaster	[70, 150]
Intersection	[100, 150]

3.1.2 pH study - solvent

As mentioned in 1.2.1, more alkaline solvents enhance the synthesis. Therefore, two water pH were tested, 6.8 pH and 9.1 pH deionized water. The alkaline water with 9.1 pH was obtained using a Miracle Max™ Royale water ionizer by Chanson, with continuous electrolysis, antibacterial filter with silver coated activated carbon, and calcium addition to alkaline water.

Our research began with the use of bunho (*Schoenoplectus lacustris*), which was the first natural source we could access to synthesize the green ZnO nanostructures. It was used at the concentrations of 0.1 g / 100 mL and 1.0 g / 100 mL (minimum and maximum, respectively), and SEM characterization was employed to reach conclusions about the size and morphology of the nanostructures generated (see figure 4).

The nanostructures obtained in the reference and with 0.1 g/ 100 mL of bunho were bigger than desired for the applications intended. The aim is to achieve nanostructures with dimensions closer to 50 nm. With higher water pH the structures were smaller than with lower pH.

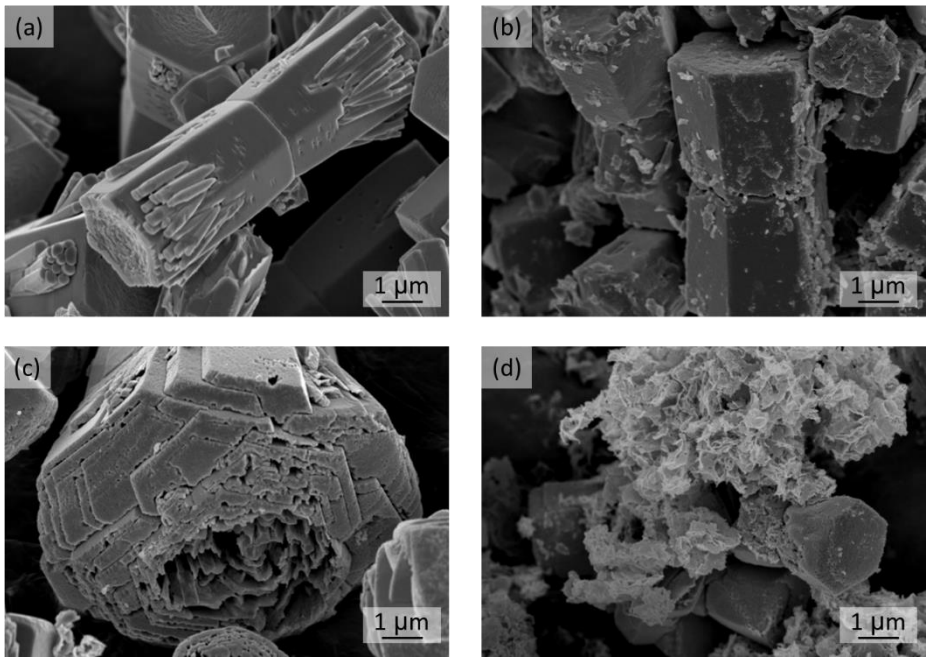

Figure 4. SEM images of: ZnO reference samples synthetized with de-ionized water with pH: a) 6.8 and b) 9; and bunho-based ZnO samples synthetized with a concentration of 1.0 g of plant extract per 100 mL of deionized water with pH: c) 6.8 and d) 9.1.

The flakes present in the samples with higher pH were more interesting than the prisms or rods, as they presented more surface area and potentially smaller sizes if not agglomerated. Their irregularity, however, makes it difficult to control their behavior and possible interactions during application.
Preliminary SEM images (see Figure 5) of ZnO nanoparticles synthesized with 1.0 g of bunho revealed better results than with less natural extract quantity, resulting in nanoparticles with dimensions around 50 nm. Overall, the samples with a solvent with higher pH present smaller structures, which enhances the synthesis, so de-ionized water with 9.1 pH will be favored in the rest of the work.

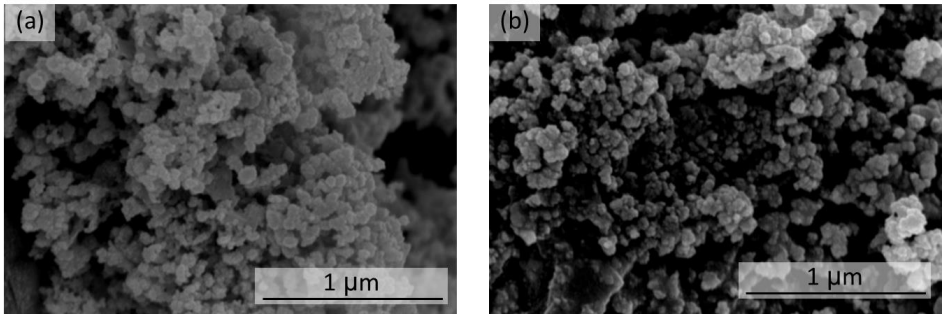

Figure 5. SEM images of bunho-based ZnO samples synthetized with zinc acetate and a concentration of 1.0 g of plant extract per 100 mL of deionized water with pH: a) 6.8 and b) 9.1, in a MW at 140ºC for 20 minutes.

3.1.3 Concentration of reagents

Concentrations of natural extracts between 0.1 g and 1.0 g per 100 mL of solvent were tested for the synthesis of ZnO nanostructures. For this section, barbatimão was used in the following concentrations: 0.1, 0.3, 0.5, 0.7, and 1.0 g per 100 mL of solvent. Considering the conclusions from the previous

chapters the temperature of synthesis was 140 ºC and the solvent was deionized water with 9.1 pH. The results can be found in Table 2.

The weight of the powder generated by the synthesis as well as the morphology and size of the nanostructures were considered to determine the optimal concentration. Logically, when more quantity of plant is used, more quantity of powder will be obtained in the synthesis, but the goal is to find an equilibrium point where the plant isn't coating too much of the ZnO, which compromises its properties and makes it unusable for certain applications, as well to economize the plant extracts. And, at the same time, we want to have enough plant that enhances the original ZnO nanostructures and contributes to their eco-friendliness.

Table 2. Summary of barbatimão-based ZnO nanostructures samples synthesized in a MW at 140 ºC for 20 minutes, for ideal concentration study.

Amount of plant extract per 100 mL of solvent (g)	Powder weight obtained per synthesis (mg)	Size (nm)	Shape
0.1	21.1	n.d.	Irregular
0.3	16.2	n.d.	Irregular, Spherical
0.5	33.6	25-31	Spherical
0.7	45.6	20-33	Spherical
1.0	51.1	26-35	Spherical

As Figure 6 suggests, the initial and second concentrations of the samples are irregularly shaped. They appear to be nanostructured, but not well-defined. They are highly agglomerated and tightly packed, so their size cannot be determined precisely. Hence, 0.1 and 0.3 g of plant extract wasn’t enough. While in the samples with 0.5, 0.7, and 1.0 g of plant extract exhibit well-defined spheres with adequate dimensions that can be used for a multitude of applications.

With XRD it is possible to analyse the contents of the samples. These samples are amorphous but with 0.5 g of barbatimão it is possible to distinguish some peaks that coincide with ZnO. The samples with higher concentrations of plants are more amorphous and don’t have as distinguishable and intense peaks. Since samples with 0.7 and 1.0 g of plant extract provide no significant advantages over sample with 0.5 g, the one with the lowest plant concentration is selected as the ideal concentration.

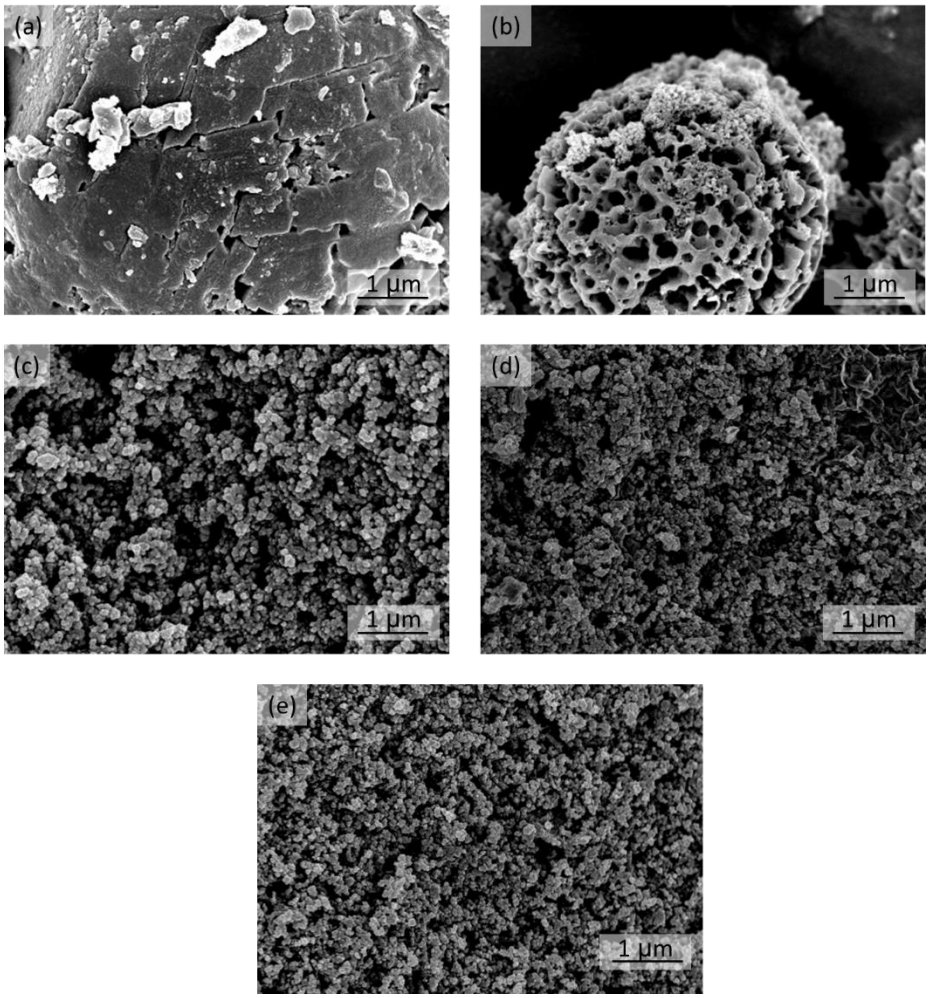

Figure 6. SEM images of plant-based ZnO samples synthesized with zinc acetate and: a) 0.1 g, b) 0.3 g, c) 0.5 g, d) 0.7 g, and e) 1.0 g of barbatimão bark extract per 100 mL of de-ionized water (9.1 pH) in a MW at 140 ºC for 20 minutes.

3.2 Plant-based nanostructures

The synthesis temperature was set at 140 ºC, the solvent was de-ionized water with a pH of 9.1, and the concentration of plant extract was 0.5 g / 100 mL of solvent, considering that the precursor concentration was constant at 1.1 g / 100 mL, we can now test all the different plant extracts to determine which one is best for the synthesis of plant-based ZnO.

Several variables were considered for this study, including the size and shape of the nanostructures with SEM, the zinc and oxygen contents using EDS analysis, the XRD peaks of the samples that correspond to the standard ZnO and our reference, as well as how much powder was generated during one synthesis.

3.2.1 Quantity

It is ideal to generate more than 25 mg of powder per synthesis to be efficient since this is the amount required for a single photocatalysis experiment. In Table 3 it can be observed that the plant extracts that belong to the bark produce more quantity of powder than wood or pine needles.

Table 3. Quantity of powder generated by one synthesis for all the different plant extracts studies, each in a concentration of 0.5 g per 100 mL of de-ionized water (9.1 pH) synthesized in a MW at 140 ºC for 20 minutes.

Plant extract	Type of extract	Powder weight (mg)
A. mearnsii	Wood	12.00
	Bark	51.30
A. melanoxylon	Wood	14.60
	Bark	28.40
P. sylvestris	Bark	44.20
P. nigra	Needle	14.40
P. pinea	Needle	20.30
P. pinaster	Needle	24.20
Schoenoplectus lacustris	Wood	15.20
Stryphnodendron	Bark	33.60

A tree's bark is generally thinner than its woody part, while both the inner bark (secondary phloem) and the wood (secondary xylem) are created by the vascular cambium layer of cells. The bark appears on the outside, where the oldest layers slough off, and the wood appears on the inside, where it accumulates as dead tissue. The moisture content of the inner bark/phloem is usually 7 to 10 times greater than that of the outer bark. In elemental analyses, bark differs from wood only in its ash components (Table 4). The phloem and the outer bark are much richer in minerals than wood (30) and pine needles. Combined, these factors may explain why bark, even when it comes from the same plant (for example with acacias), produces more powder rather than wood and needle extracts upon synthesis.

Table 4. Chemical Compounds of Spruce Wood and Bark (Ugolev 1986).

	Carbon (%)	Hydrogen (%)	Oxygen (%)	Other Elements (%)
Wood	50.0	6.0	43.5	0.5
Inner bark	51.5	5.7	38.8	4.0
Outer bark	44.4	6.4	45.4	3.8

Therefore, the samples that meet the criteria stated above belong all to bark extracts and are *A. mearnsii*, *A. melanoxylon*, *P. sylvestris*, and *Stryphnodendron* (barbatimão).

3.2.2 Dimensions and Morphology

As for size, it should be less than 50 nm, with 30 nm being the ideal diameter for clinical applications, with spherical shapes making it easier to predict and control their behavior.

Regarding the different Acacias studied, it is possible to compare the same plant from a different type of extract and the same type of extract for different plants within the same family species. In Figure 7 it is possible to examine that *A. mearnsii* tends to form spheres, though they are not discernible in the wood extract, they are very distinct in the bark extract. This makes the latter more advantageous for use in the applications. On the other hand, *A. melanoxylon*, both bark and wood extracts, is characterized by flake-like structures that are quite large.

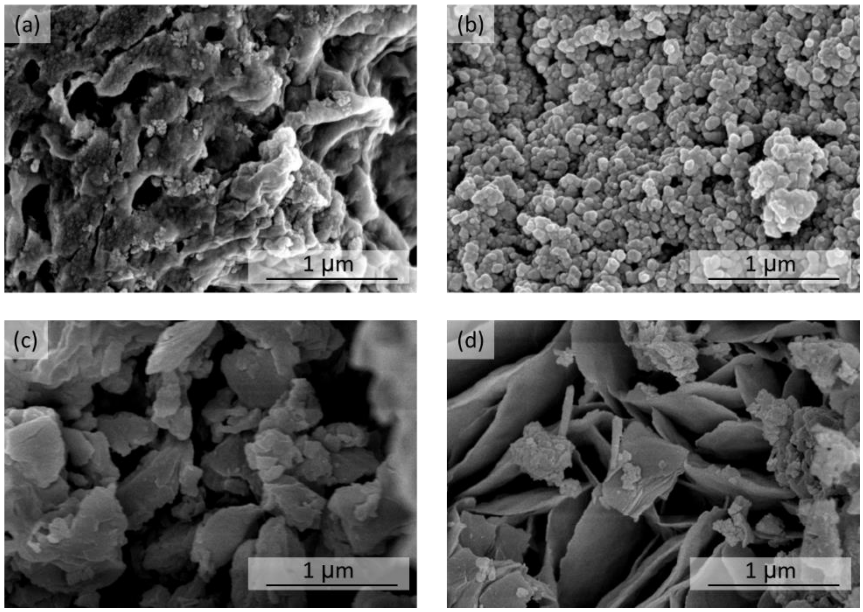

Figure 7. SEM images of plant-based ZnO samples synthesized with zinc acetate and 0.5 g of: a) *A. mearnsii* wood, b) *A. mearnsii* bark, c) *A. melanoxylon* wood, and d) *A. melanoxylon* bark extracts, per 100 mL of de-ionized water (9.1 pH) in a MW at 140 ºC for 20 minutes.

In Figure 8, it is possible to see pine-based nanostructures. In the first one, *P. sylvestris* is the only sample of the four pines that originate from bark extract, while the other pines are from pine needles, and the distinction is clear as it has perfect nanospheres. In contrast, *P. nigra*, *pinea*, and *pinaster* result in structures that aren't possible to define regarding their shape and size.

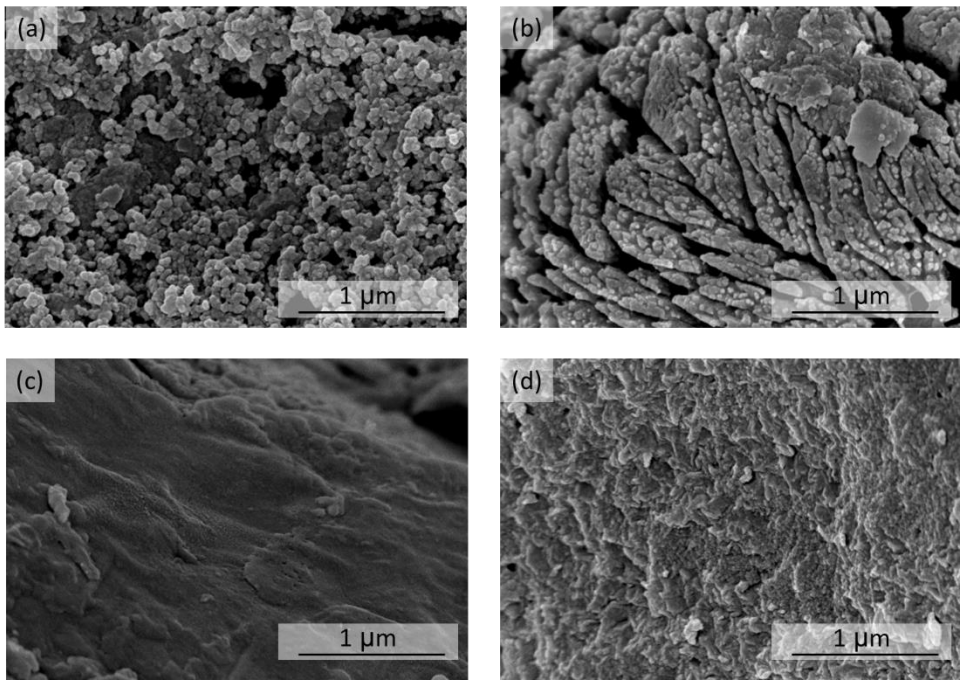

Figure 8. SEM images of plant-based ZnO samples synthesized with zinc acetate and 0.5 g of: a) *P. sylvestris* bark, b) *P. nigra*, c) *P. pinea*, and d) *P. pinaster* needle extracts, per 100 mL of de-ionized water (9.1 pH) in a MW at 140 ºC for 20 minutes.

Lastly, *Schoenoplectus lacustris* (bunho) wood extract resulted in flake-like structures that even though have small sizes, are irregular and too agglomerated, while *Stryphnodendron* (barbatimão) bark extract results in well-defined spheres with an appropriate size in the nanoscale, as can be seen in Figure 9.

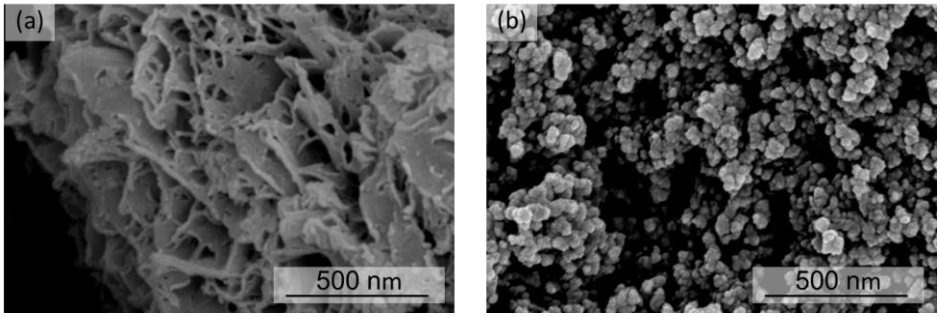

Figure 9. SEM images of pant-based ZnO samples synthesized with zinc acetate and 0.5g of: a) bunho wood and b) barbatimão bark extracts per 100 mL of de-ionized water (9.1 pH) in a MW at 140ºC for 20 minutes.

Regardless of the type of plant that is being referred to, bark-type extracts provide better results in this synthesis than wood or needles. Table 5 consists of an overview of all the data collected from the SEM analysis.

Table 5. Summary of the samples' shape and size with SEM characterization.

Plant extract	Type of extract	Shape	Size (nm)
A. mearnsii	Wood	Irregular	n.d.
	Bark	Spherical	52.6
A. melanoxylon	Wood	Irregular	n.d.
	Bark	Irregular	n.d.
P. sylvestris	Bark	Spherical	36.3
P. nigra	Needle	Irregular, some spheres	39.4
P. pinea	Needle	Irregular	n.d.
P. pinaster	Needle	Irregular, some spheres	18.6
Schoenoplectus lacustris	Wood	Irregular	n.d.
Stryphnodendron	Bark	Spherical	27.2

Out of the four acacia samples, *A. mearnsii* bark extract shows the best shape and size. Regarding the pines, *P. sylvestris* bark extract is the best. Lastly, *Stryphnodendron* bark extract also meets the criteria. Therefore, these three samples will continue forward in the study.

3.2.3 ZnO content

To evaluate if there is ZnO in the plant-based samples, XRD characterization was used to study the peaks associated with ZnO.

In Figure 10 the plots that belong to *A. mearnsii*, *P. sylvestris*, and *Stryphnodendron* bark extracts based ZnO nanostructures can be observed. In the last two plant extracts, there is a slight curve in the beginning of the plot (even after baseline calibration), it can indicate that the sample is mostly amorphous, which is normal because of the plant coating. The contrast between acacia and barbatimão can be seen that by the distinctive peaks present in barbatimão sample that coincide with the ZnO ones (even if they don't match in intensity), that don't appear in the acacia sample. The pine sample hasn’t the characteristic curve of amorphous sample, and the peaks are clearly distinctive.

Consequently, the last sample barbatimão bark extract was the selected one to continue forward to the application's tests since it meets the criteria of this study, and it represents a good opportunity to enrich the literature with more data about this natural extract when compared with acacias or pines that are already more common in the literature.

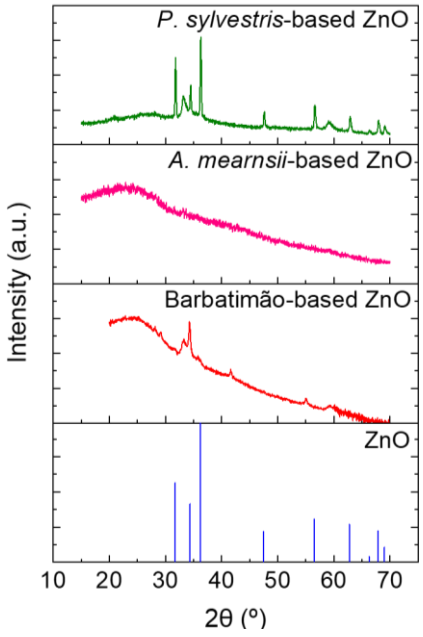

Figure 8. XRD patterns of standard ZnO and plant-based samples with *P. sylvestris*, *A. mearnsii*, and Barbatimão, synthesized with zinc acetate and 0.5 g of bark extracts per 100 mL of de-ionized water (9.1 pH), in a MW at 140 ºC for 20 minutes.

With EDS it was possible to evaluate the zinc and oxygen content present in the samples. In Figure 11, the EDS layered image of the ZnO reference on the right shows a stronger zinc signal than that of the plant-based ZnO on the left, which may be due to the plant coating at the nanostructure's core.

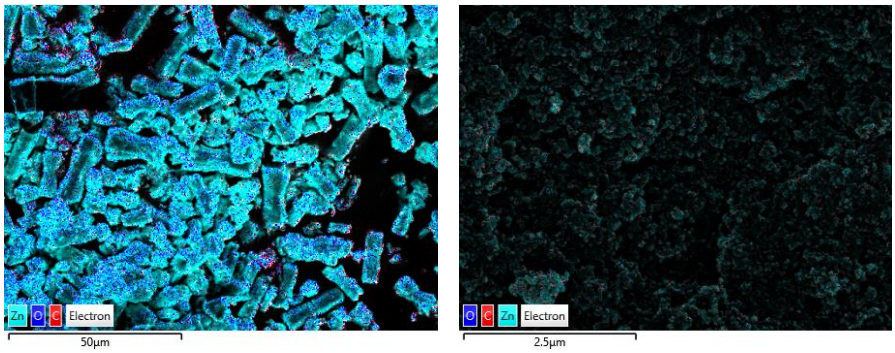

Figure 9. EDS layered image of ZnO reference and barbatimão-based ZnO samples, synthesized with de-ionized water (pH 9.1) and zinc acetate in a MW at 140 ºC for 20 minutes.

More accurately, the atomic percentage is the number of atoms of that element, at that weight percentage, divided by the total number of atoms in the sample multiplied by 100, and can be found in Table 6. The aim is to find partially equal parts of zinc and oxide. It may be impossible to adhere strictly to these criteria because of the plant's coating.

Table 6. Overview of the atomic percentage of oxygen and zinc in the ZnO reference and plant-based ZnO with barbatimão bark extract samples, synthesized in a MW at 140 ºC for 20 minutes.

Sample	Atomic %	
	O	Zn
ZnO reference	50.15	49.85
Barbatimão-based ZnO	57.86	42.14

3.3 Photocatalytic activity via RhB degradation

Based on the VIS absorption spectrum of barbatimão-based ZnO nanopowder, Figure 12, it exhibits high absorption in the 200 - 340 nm wavelength range. The barbatimão-based ZnO had a very dark brown color that made it impossible for the band gap energy to be calculated because the nanopowder hardly reflected light.

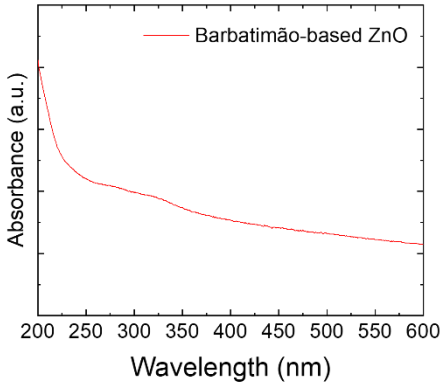

Figure 10. Absorbance plot of barbatimão-based ZnO nanostructures synthesized with de-ionized water (9.1 pH) and zinc acetate in a MW at 140ºC for 20 minutes.

An overview of all the measures taken to evaluate the photocatalytic activity of the green ZnO nanostructures can be found in Figure 13.

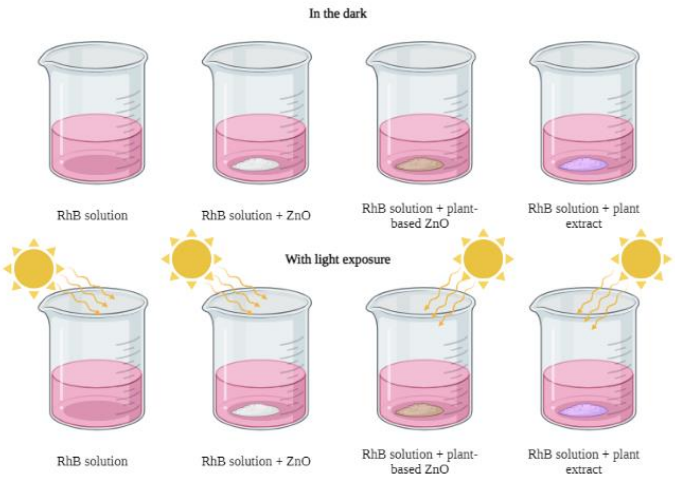

Figure 11. Schematics of sample distribution used in the photocatalysis experiments. Created in BioRender.com

In general, organic dyes obey the apparent first-order kinetics which supports the general Langmuir-Hinshelwood mechanism (34):

$$r = \frac{-dC}{dt} = \frac{kKC}{1} + KC \quad (2)$$

where r is the degradation rate of the reactant, C represents the concentration of the reactant, t is the illumination time, K is the adsorption coefficient of the reactant and k is the reaction rate constant. If C is very small, then the above equation can be written as:

$$ln\left(\frac{C_0}{C}\right) = kKt \approx k_{app}t \quad (3)$$

The photocatalytic degradation efficiency, at various time intervals, has been evaluated using the formula (35):

$$\%\ of\ degradation = \left(\frac{C_0 - C}{C_0}\right) \times 100 = \left(\frac{A_0 - A}{A_0}\right) \times 100 \quad (4)$$

where C_0 is the initial concentration, and C is the concentration corresponding to different time intervals, t. Similarly, A_0 denotes the initial absorbance whereas, A represents the absorbance at time, t. Hence, the degradation of RhB will be given by:

$$\%\ of\ degradation = \left(\frac{A_0 - A}{A_0}\right) \times 100 \quad (5)$$

The RhB photodegradation was observed by monitoring the evolution of the absorption band intensity at 554 nm upon continued exposure. The efficiency of dye degradation with the ZnO reference, plant-based ZnO and the plant extract, in three and a half hours, was calculated from equation 5. In this period, the ZnO reference degraded, about, 13% of the RhB dye, while the barbatimão-based ZnO samples displayed more efficiency, roughly 59%. It was also possible to investigate with only the barbatimão bark extract, with approximately 23% of dye degradation. A rundown of the data collected can be seen in Table 7.

Table 7. Dye degradation efficiency with photocatalysis experiments data of ZnO reference and plant-based ZnO, using equation 5.

	ZnO Reference	Barbatimão-based ZnO	Barbatimão bark extract
A_0	0.96695	0.85586	0.58900
$A_{3.5\ h}$	0.83874	0.35033	0.45359
Dye degradation (%)	13.259	59.067	22.989

Figure 14, on the left side, presents the RhB photodegradation in the presence of ZnO reference, barbatimão-based ZnO, and barbatimão bark extract. On the right, it is the degradation rate for each sample and the reusability of the barbatimão-based ZnO nanostructures.

Both in the plant-based ZnO and the plant extract samples, the absorbance doesn't begin as close to 100%, which is what happens with the ZnO reference, as expected. This reaction may be accelerated by plant phytochemicals, especially tannin, which happens as soon as the powder is combined with the RhB solution. It takes about half an hour or more to reach the absorption-desorption equilibrium, but with plant extracts, this can't be applied. Upon the mixture of the ingredients, the plant-based ZnO

samples start to degrade the dye right away and when it is time to put the sample in the cuvette to collect the spectrum data, the absorbance is already on its way down at t_0.

The experiment with only the plant extract has a dye degradation capability comparable to the ZnO reference, although not as effective the combination of both. Therefore, it is expected that ZnO and the plant extract together result in a much faster photodegradation.

To study the recyclability of the barbatimão-based ZnO nanopowder after one experiment, they were cleaned with de-ionized water and dried overnight at 80ºC to be tested again in a second cycle in a new RhB solution. Other possible cleaning treatment to experiment with in the future would be to do a UV treatment to the nanopowder to completely degrade the remaining RhB that may be attached to the nanostructures. The results showed a reduction in the degradation of dye, from 59% in the first cycle to 42% in the second. Thus, it is possible to reuse the nanopowder, though their photocatalytic activity will decrease with each use.

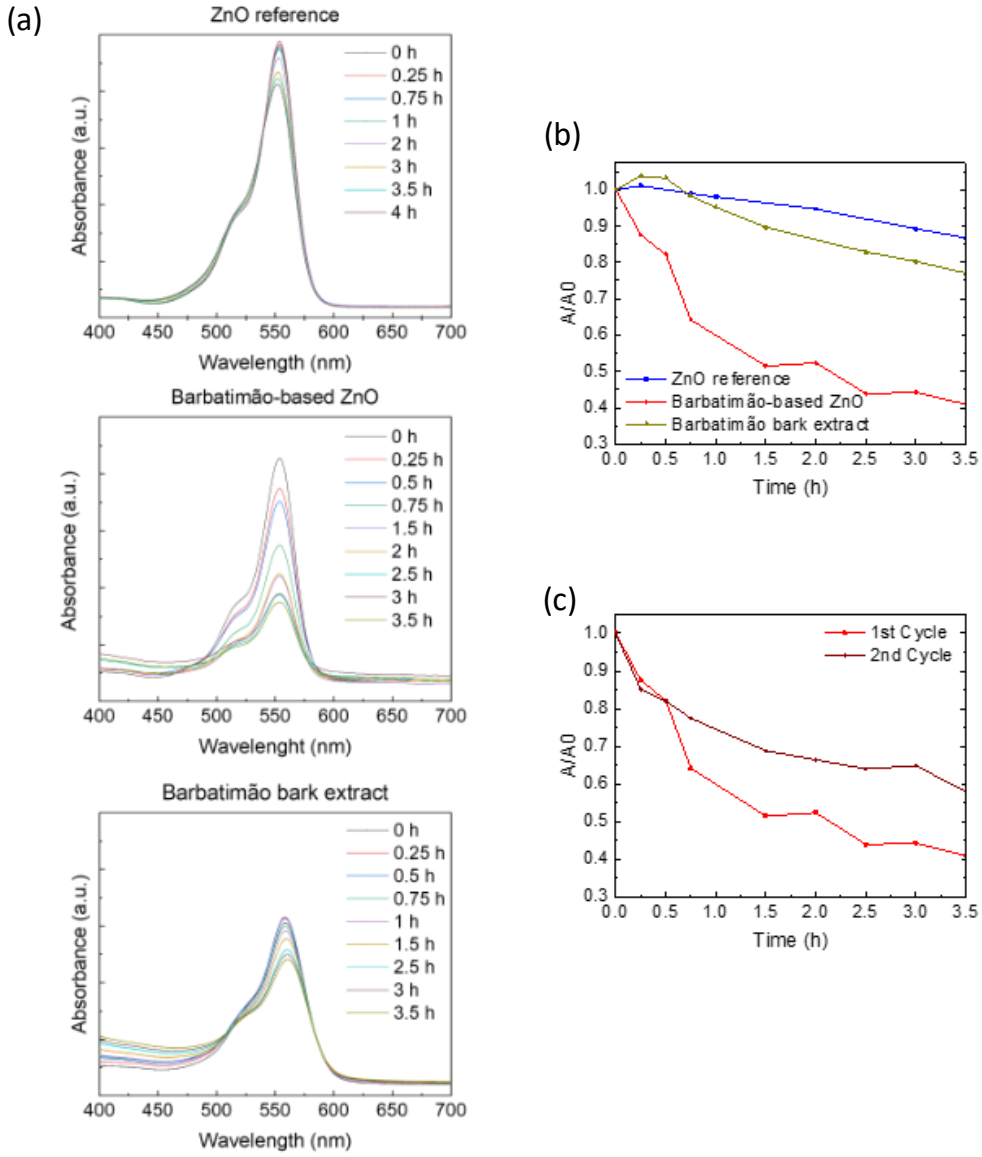

Figure 12. Photocatalytic degradation of RhB over time in the presence of a) ZnO reference (without natural extracts), barbatimão-based ZnO nanostructures synthesized with de-ionized water and zinc acetate at 140 ºC, and barbatimão bark extract, under a VIS radiation; b) absorbance versus exposure time for different photocatalysts; c) cycling runs in the photocatalytic degradation of a RhB solution in the presence of plant-based ZnO nanostructures.

To understand if this is a photocatalysis reaction instead of just a catalyst one by the plant-based ZnO nanostructures, the samples were subjected to experiments both in the dark and with light irradiation. It can be stated, from the results shown in Table 8, that light exposure enhances this reaction. The dye degradation efficiency is higher with light exposure than without it. There is still a small dye degradation in the dark, which is due to the presence of the plant that inherently contributes to the reaction, but it is much higher in light. There were multiple replicate experiments, which heightened the level of reproducibility in the results.

Table 8. Comparison between the dye degradation efficiency of barbatimão-based ZnO in the dark and with light exposure.

Barbatimão-based ZnO	In the dark	With light exposure
A_0	0.86855	0.85586
$A_{3.5\ h}$	0.73906	0.35033
Dye degradation (%)	12.949	59.067

It is important to remark that we are working with many variables that influence this data. For instance, the time it takes to transport the samples from the chemical to the optoelectronics laboratories, and the local place with the best direct sunlight when natural light was used. It is also impossible to stop the reactions from happening during the time the measurement are being taken, and when we are doing more than one sample at once this period extends. Therefore, the time stamps aren't absolutely uniform. During the light irradiation, the samples tend to overheat, even with refrigerating systems, which may lead to the evaporation of a small portion of the solution that may cause irregularities in the results.

3.4 *E. coli* inactivation by photocatalyst

A calibration curve for the positive control (bacteria without any treatment) was done with light exposure with different wavelengths. The graph with the results is in Figure 15, and the LED wavelength chosen of 365 nm is within the interval therefore it's use is appropriate.

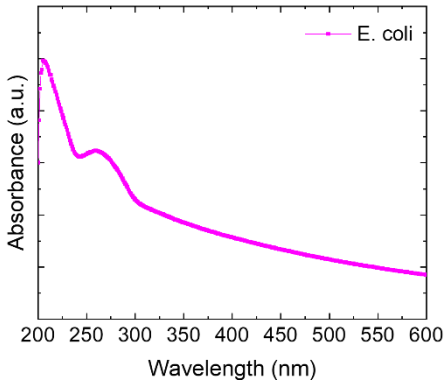

Figure 13. *E. coli* control calibration curve.

The *E. coli* inactivation by photocatalyst tests can be summarized in Figure 16. The first control of bacteria in the dark was collected at the beginning and at the end of the experiment, after 20 minutes (t_0 and t_{20}, respectively), and the bacteria control with LED irradiation was collected with a 5-minute interval between collections. The goblets with plant-based ZnO powder were collected within smaller time periods (30 seconds).

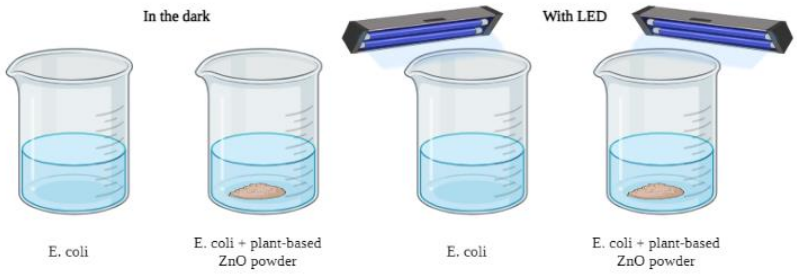

Figure 14. Schematics of sample distribution used in the photocatalytic experiment on the *E. coli* inactivation assay. Created in BioRender.com

Following the tests, the various samples collected during the experiment were diluted as suggested in Figure 17. Then, they were incubated on to the plates for later counting.

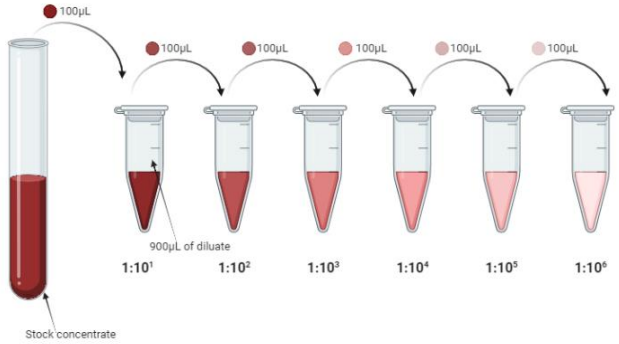

Figure 15. Schematics of initial samples dilutions. Created in BioRender.com.

The microorganism plate counting method was used to analyse the colonies that grew after the experiment, following the equation:

$$CFU/mL = \frac{No.of\ colonies * dilution\ factor}{volume\ of\ culture\ plate} \quad (6)$$

The initial bacterial concentration was of 4.70×10^6 for a dilution of $1{:}10^3$ and the bacterial counts before and after treatment can be found in Table 9. Granting, the bacterial colonies couldn't be counted with the same dilutions for all the tests.

Table 9. Bacterial counts before and after treatment.

Bacterial Counts (CFU/mL)	Dark		LED	
	E. coli	*E. coli* + plant-based ZnO	*E. coli*	*E. coli* + plant-based ZnO
t_0	4.20×10^6	3.15×10^6	4.40×10^6	4.73×10^6
$t_{20\ min}$	5.80×10^6	5.72×10^6	2.13×10^5	3.66×10^6

An overview of the bacteria colonies over the time of the experiment for the different conditions can be found in Figure 18, to evaluate the reduction in bacterial viability. Only the control with bacteria and no LED has a proportional relationship between the number of bacteria and the time spent on the

experiment. This direct proportion indicates that the bacteria are multiplying over time since there are no factors to inhibit them. However, when the LED and nanostructure variables are inserted, this behavior is irregular and incoherent during the experiment.

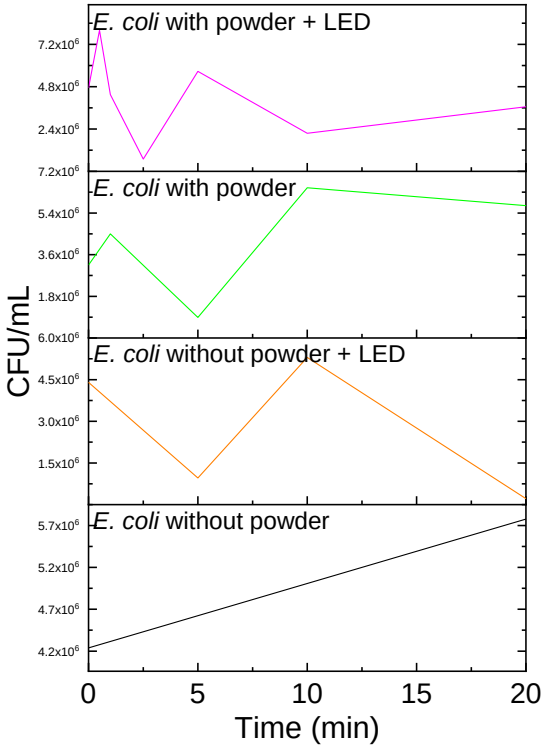

Figure 16. Bacterial inactivation assay results with barbatimão-based ZnO nanostructures powder and LED irradiation.

When only considering the initial and final time stamps of the experiment, *E. coli* with LED, with and without powder, are the only cases where colony formation diminishes. Therefore, it isn't possible to conclude that plant-based nanostructures play a role in inhibiting bacteria.

The results obtained weren't conclusive, so it's not possible to determine that the plant-based nanostructures have antibacterial potential. However, more studies could be done to test different bacteria and different conditions.

Other considerations may also have influenced these results, explicitly contamination in the lab hotte since the control plaque had 58 colonies, which is already a significant number. Nonetheless, even with the possibility of contamination in the working environment, there wasn't any relationship between bacteria inactivation and the presence of plant-based ZnO nanostructure with or without LED irradiation. There is also the complexity of nanostructure-bacteria interactions that should be considered and better understood since it can depend on various factors.

4

CONCLUSIONS AND FUTURE PERSPECTIVES

In the quest to harness the potential of plant-based ZnO nanostructures, this study embarked on a journey of discovery, exploration, and application. By merging the natural world's offerings with cutting-edge technology, we endeavored to uncover novel solutions for water treatment and antibacterial applications. This journey led us through the domains of green synthesis, characterization, and multifaceted testing.

Zinc oxide nanoparticles were successfully fabricated using the green synthesis facilitated method using bark extracts from *Stryphnodendron, A. mearnsii, A. melanoxylon,* and *P. sylvestris*, wood extracts from *A. mearnsii* and *A. melanoxylon,* and needle extracts from *P. nigra, P. pinea,* and *P. pinaster*.

Considering the intensive study of all the different natural extracts, A. *mearnsii, P. sylvestris*, and *Stryphnodendron* bark extracts showed the best results during the study. It is also important to note that bark type of extracts was the most promising. Still, barbatimão (*Stryphnodendron*) bark extract can be reflected as the most pertinent because of its rich tannin content that provides more potential and other intrinsic properties for a variety of applications. Besides, the literature on the green synthesis of nanostructures could benefit from additional documentation on this plant.

The study reports a non-toxic, inexpensive, and environmentally friendly method of nanoparticle synthesis. The optimal synthesis included natural bark extracts, zinc nitrate as the precursor, and de-ionized water with 9.1 pH as the solvent, in a microwave at 140 ºC for 20 min, and 100W power.

In the barbatimão-based ZnO nanostructures, the presence of nanoparticles was confirmed by SEM analysis revealing the compound as zinc oxide whose composition was provided by EDS and RDX analysis. As a photocatalyst, it demonstrated 59% dye degradation within 3.5 hours, whereas the ZnO reference was only 13%, demonstrating its practical significance for potential applications in water treatment for pollutant degradation.

Unfortunately, the *E. coli* inactivation by the optimized plant-based nanostructures did not yield conclusive results, no correlation could be found. The initial results did not match the hypothesis of antibacterial activity, but some experimental variability was encountered during the assays that were challenging.

In future studies, it may be interesting to vary other factors such as test conditions, nanostructure concentrations, and bacterial strains used. Only after that, can it be concluded with certainty that the lack of observed antibacterial activity may not necessarily imply the absence of all antibacterial potential.

While the initial hypothesis of antibacterial activity was not supported by the current experiments, further investigation is needed to reach a definitive conclusion. Various tests and conditions can be

explored to determine whether the nanostructures have any antibacterial potential, including tests with different bacterial strains, concentrations, and exposure times. Other directions can also be followed, such as trying UV instead of VIS and exploring other studies that have already been done in iBET (e.g., UV degradation kinetics and modeling of pharmaceutical compounds in laboratory grade and surface water via direct and indirect photolysis at the appropriate wavelength, oxidation of pharmaceuticals during ozonation and advanced oxidation processes, or quantifying the hydroxyl radical/ozone ratios during ozonation processes).

Despite the absence of conclusive antibacterial activity results, they underline the significance of the present study in advancing the knowledge of plant-based ZnO nanostructures and their possible applications. The successful photocatalytic activity results have tangible implications for water treatment and pollution control, demonstrating the value of these research outcomes.

As this chapter is closed, it's important to recognize that science thrives on both successes and challenges. While the anticipated antibacterial prowess of our nanostructures did not manifest as expected, this work illuminated new paths for investigation. The significance of this research, highlighted by the successful photocatalytic prowess of our ZnO nanostructures, inspires further inquiries, collaborations, and breakthroughs in sustainable and impactful technologies.

BIBLIOGRAPHY

1. Aremu OH, Akintayo CO, Naidoo EB, Nelana SM, Ayanda OS. Synthesis and applications of nano-sized zinc oxide in wastewater treatment: a review. Int J Environ Sci Technol 2021 1810 [Internet]. 2021 Feb 9 [cited 2023 Jun 30];18(10):3237–56. Available from: https://link.springer.com/article/10.1007/s13762-020-03069-1
2. Yang Y, Sik Ok Y, Kim K-H, Kwon EE, Tsang YF. Occurrences and removal of pharmaceuticals and personal care products (PPCPs) in drinking water and water/sewage treatment plants: A review. 2017 [cited 2023 Jun 30]; Available from: http://dx.doi.org/10.1016/j.scitotenv.2017.04.102
3. Liu J-L, Wong M-H. Pharmaceuticals and personal care products (PPCPs): A review on environmental contamination in China. 2013 [cited 2023 Jun 30]; Available from: http://dx.doi.org/10.1016/j.envint.2013.06.012
4. Ameen S, Shaheer Akhtar M, Nazim M, Shin H-S. Rapid photocatalytic degradation of crystal violet dye over ZnO flower nanomaterials. 2013 [cited 2023 Jun 30]; Available from: http://dx.doi.org/10.1016/j.matlet.2013.01.034
5. Lun Ang W, Wahab Mohammad A, Hilal N, Leo CP. A review on the applicability of integrated/hybrid membrane processes in water treatment and desalination plants. 2014 [cited 2023 Jun 30]; Available from: http://dx.doi.org/10.1016/j.desal.2014.03.008
6. Wang B, Wan Y, Gao Y, Zheng G, Yang M, Wu S, et al. Occurrences and Behaviors of Naphthenic Acids in a Petroleum Refinery Wastewater Treatment Plant. 2015 [cited 2023 Jun 30]; Available from: https://pubs.acs.org/sharingguidelines
7. Antonio M, Cardenas R, Ali I, Lai FY, Dawes L, Thier R, et al. Removal of micropollutants through a biological wastewater treatment plant in a subtropical climate, Queensland-Australia. 2016;
8. Venzke CD, Rodrigues MAS, Giacobbo A, Bacher LE, Lemmertz IS, Viegas C, et al. Application of reverse osmosis to petrochemical industry wastewater treatment aimed at water reuse. Manag Environ Qual An Int J. 2017;28(1):70–7.
9. Ji Z. Treatment of heavy-metal wastewater by vacuum membrane distillation: Effect of wastewater properties. IOP Conf Ser Earth Environ Sci [Internet]. 2018 Jan 30 [cited 2023 Jun 30];108(4). Available from: https://www.researchgate.net/publication/322810401_Treatment_of_heavy-metal_wastewater_by_vacuum_membrane_distillation_effect_of_wastewater_properties
10. Pei Y, Wang L, Huang L, - al, Rezki M, Luh Wulan Septiani N, et al. IOP Conference Series: Earth and Environmental Science Ion Exchange Resin on Treatment of Copper and Nickel Wastewater Review-Recent Advance in Multi-Metallic Metal Organic Frameworks (MM-MOFs) and Their Derivatives for Electrochemical Biosensor Application Ion Exchange Resin on Treatment of Copper and Nickel Wastewater. IOP Conf Ser Earth Environ Sci. 2017;94:12122.
11. Gopal K, Swarupa Tripathy S, Luc Bersillon J, Dubey SP. Chlorination byproducts, their

toxicodynamics and removal from drinking water. J Hazard Mater. 2007;140:1–6.
12. Preparation and characterization of barium incorporated zinc oxide nanoparticles [Internet]. [cited 2022 Oct 29]. Available from: https://docplayer.net/214022800-Preparation-and-characterization-of-barium-incorporated-zinc-oxide-nanoparticles.html
13. Kumar SS, Venkateswarlu P, Rao VR, Rao GN. Synthesis, characterization and optical properties of zinc oxide nanoparticles. Int Nano Lett 2013 31 [Internet]. 2013 May 7 [cited 2022 Oct 29];3(1):1–6. Available from: https://link.springer.com/article/10.1186/2228-5326-3-30
14. Agarwal H, Venkat Kumar S, Rajeshkumar S. A review on green synthesis of zinc oxide nanoparticles – An eco-friendly approach. Resour Technol [Internet]. 2017;3(4):406–13. Available from: https://doi.org/10.1016/j.reffit.2017.03.002
15. Kessler R. Engineered Nanoparticles in Consumer Products: Understanding a NewIngredient. Environ Health Perspect [Internet]. 2011 Mar [cited 2022 Oct 29];119(3):A120. Available from: /pmc/articles/PMC3060016/
16. Augustine R, Hasan A. Emerging applications of biocompatible phytosynthesized metal/metal oxide nanoparticles in healthcare. J Drug Deliv Sci Technol [Internet]. 2020;56(December 2019):101516. Available from: https://doi.org/10.1016/j.jddst.2020.101516
17. Larson RA. The antioxidants of higher plants. Phytochemistry. 1988 Jan 1;27(4):969–78.
18. Naseer M, Aslam U, Khalid B, Chen B. Green route to synthesize Zinc Oxide Nanoparticles using leaf extracts of Cassia fistula and Melia azadarach and their antibacterial potential. Sci Rep [Internet]. 2020 Dec 1 [cited 2022 Dec 11];10(1). Available from: https://pubmed.ncbi.nlm.nih.gov/32493935/
19. Karmous I, Taheur F Ben, Zuverza-Mena N, Jebahi S, Vaidya S, Tlahig S, et al. Phytosynthesis of Zinc Oxide Nanoparticles Using Ceratonia siliqua L. and Evidence of Antimicrobial Activity. Plants. 2022;11(22):1–15.
20. Makarov V V., Love AJ, Sinitsyna O V., Makarova SS, Yaminsky I V., Taliansky ME, et al. "Green" Nanotechnologies: Synthesis of Metal Nanoparticles Using Plants. Acta Naturae [Internet]. 2014 [cited 2022 Dec 11];6(1):35. Available from: /pmc/articles/PMC3999464/
21. Doan Thi TU, Nguyen TT, Thi YD, Ta Thi KH, Phan BT, Pham KN. Green synthesis of ZnO nanoparticles using orange fruit peel extract for antibacterial activities. RSC Adv. 2020;10(40):23899–907.
22. Mahdi Ismail SM, Ahmed SM, Abdulrahman AF, AlMessiere MA. Characterization of green synthesized of ZnO nanoparticles by using pinus brutia leaves extracts. J Mol Struct. 2023 May 15;1280:135063.
23. Gatou MA, Lagopati N, Vagena IA, Gazouli M, Pavlatou EA. ZnO Nanoparticles from Different Precursors and Their Photocatalytic Potential for Biomedical Use. Nanomater 2023, Vol 13, Page 122 [Internet]. 2022 Dec 26 [cited 2023 Apr 4];13(1):122. Available from: https://www.mdpi.com/2079-4991/13/1/122/htm
24. Souza-Moreira TM, Queiroz-Fernandes GM, Pietro RCLR. Stryphnodendron Species Known as "Barbatimão": A Comprehensive Report. Mol A J Synth Chem Nat Prod Chem [Internet]. 2018 [cited 2023 Feb 9];23(4). Available from: /pmc/articles/PMC6017227/
25. Scalbert A. Antimicrobial properties of tannins. Phytochemistry. 1991 Jan 1;30(12):3875–83.
26. Dobson RS, Burgess JE. Biological treatment of precious metal refinery wastewater: A review. Miner Eng. 2007 May;20(6):519–32.
27. Saravanan R, Gupta VK, Narayanan V, Stephen A. Comparative study on photocatalytic activity of ZnO prepared by different methods. J Mol Liq [Internet]. 2013;181:133–41. Available from: http://dx.doi.org/10.1016/j.molliq.2013.02.023
28. Tuttle AR, Trahan ND, Son MS. Growth and Maintenance of Escherichia coli Laboratory Strains. Curr Protoc [Internet]. 2021 Jan 20 [cited 2023 Aug 15];1(1). Available from: http://openwetware.org/index.php?title=E._coli_genotypes&oldid=577711
29. Park S, Baker JO, Himmel ME, Parilla PA, Johnson DK. Cellulose crystallinity index: Measurement techniques and their impact on interpreting cellulase performance. Biotechnol Biofuels [Internet]. 2010 May 24 [cited 2023 Sep 4];3(1):1–10. Available from: https://biotechnologyforbiofuels.biomedcentral.com/articles/10.1186/1754-6834-3-10

30. Pásztory Z, Ronyecz Mohácsiné I, Gorbacheva G, Börcsök Z. The Utilization of Tree Bark.
31. Sun J, Wang H, Zhang Y, Zheng Y, Xu Z, Liu R. Structure and luminescent properties of electrodeposited Eu 3 +-doped CaF2 thin films. Thin Solid Films. 2014;562:478–84.
32. Kumar RGA, Hata S, Gopchandran KG. Diethylene glycol mediated synthesis of Gd2O3:Eu3+ nanophosphor and its Judd–Ofelt analysis. Ceram Int. 2013 Dec 1;39(8):9125–36.
33. Raji R, Gopchandran KG. ZnO nanostructures with tunable visible luminescence: Effects of kinetics of chemical reduction and annealing. 2017 [cited 2023 Sep 6]; Available from: http://dx.doi.org/10.1016/j.jsamd.2017.02.002
34. Ohtani B. Photocatalysis by inorganic solid materials: Revisiting its definition, concepts, and experimental procedures. Adv Inorg Chem. 2011 Jan 1;63:395–430.
35. Chen CY. Photocatalytic degradation of azo dye reactive orange 16 by TiO2. Water Air Soil Pollut [Internet]. 2009 Sep 30 [cited 2023 Sep 8];202(1–4):335–42. Available from: https://link.springer.com/article/10.1007/s11270-009-9980-4
36. Ashwini J, Aswathy TR, Rahul AB, Thara GM, Nair AS. Synthesis and characterization of zinc oxide nanoparticles using acacia caesia bark extract and its photocatalytic and antimicrobial activities. Catalysts. 2021;11(12).
37. Bajpai SK, Jadaun M, Tiwari S. Synthesis, characterization and antimicrobial applications of zinc oxide nanoparticles loaded gum acacia/poly(SA) hydrogels. Carbohydr Polym. 2016 Nov 20;153:60–5.
38. Rasha E, Monerah A, Manal A, Rehab A, Mohammed D, Doaa E. molecules Biosynthesis of Zinc Oxide Nanoparticles from Acacia nilotica (L.) Extract to Overcome Carbapenem-Resistant Klebsiella Pneumoniae. 2021 [cited 2023 Feb 24]; Available from: https://doi.org/10.3390/molecules26071919
39. Irfan M, Munir H, Ismail H. Characterization and fabrication of zinc oxide nanoparticles by gum Acacia modesta through green chemistry and impregnation on surgical sutures to boost up the wound healing process. Int J Biol Macromol [Internet]. 2022;204(November 2021):466–75. Available from: https://doi.org/10.1016/j.ijbiomac.2022.02.043
40. Irfan M, Munir H, Ismail H. Characterization and fabrication of zinc oxide nanoparticles by gum Acacia modesta through green chemistry and impregnation on surgical sutures to boost up the wound healing process. Int J Biol Macromol. 2022 Apr 15;204:466–75.
41. Hayat S, Ashraf A, Zubair M, Aslam B, Siddique MH, Khurshid M, et al. Biofabrication of ZnO nanoparticles using Acacia arabica leaf extract and their antibiofilm and antioxidant potential against foodborne pathogens. PLoS One [Internet]. 2022;17(1 Januray):1–18. Available from: http://dx.doi.org/10.1371/journal.pone.0259190
42. Nhu VTT, Dat ND, Tam LM, Phuong NH. Green synthesis of zinc oxide nanoparticles toward highly efficient photocatalysis and antibacterial application. Beilstein J Nanotechnol 1394 [Internet]. 2022 Oct 7 [cited 2023 Aug 7];13(1):1108–19. Available from: https://www.beilstein-journals.org/bjnano/articles/13/94
43. Velmurugan P, Park JH, Lee SM, Jang JS, Yi YJ, Han SS, et al. Phytofabrication of bioinspired zinc oxide nanocrystals for biomedical application. Artif Cells, Nanomedicine Biotechnol [Internet]. 2016 Aug 17 [cited 2023 Aug 7];44(6):1529–36. Available from: https://www.tandfonline.com/doi/abs/10.3109/21691401.2015.1058811
44. Honarmand M, Amini M, Iranfar A, Naeimi A. Green Synthesis of ZnO/SnO2 Nanocomposites Using Pine Leaves and Their Application for the Removal of Heavy Metals from Aqueous Media. J Clust Sci [Internet]. 2022 Jan 1 [cited 2023 Aug 7];33(1):301–10. Available from: https://link.springer.com/article/10.1007/s10876-020-01960-y

A

SUPPORT INFORMATION

A.1 State of the Art

Table 10. Summary of literature on the green synthesis of ZnO nanostructures with plant extracts.

Plant extract	Synthesis	Precursor	Size and Shape	Application	Refs.
		Acacia			
Acacia caesia (bark)	65 ºC for 40min + calcination 400 ºC for 2h	Zinc nitrate hexahydrate	32nm Hexagonal	Photocatalytic and antimicrobial	(36)
Gum acacia	60 ºC for 2h	Zinc sulphate	40-60 nm	Antimicrobial	(37)
Gum acacia	70 ºC for 3h + calcination 500 ºC for 3h	Zinc acetate	16 nm Hexagonal	Photocatalytic	
Acacia nilotica (fruit)	80 °C for 2 h + 80 °C for 2 h + calcination 400 °C for 2 h	Zinc nitrate	94 nm Hexagonal, irregular, spherical	Antimicrobial	(38)
Acacia moringa oleifera	70 ºC for 4h + calcination 400 ºC for 4 h	Zinc nitrate	n.d.	Antibacterial	(39)
Acacia modesta	70 ºC for 4h	Zinc nitrate hexahydrate	70 nm Rods	Antibacterial, wound healing	(40)
Acacia arabica (leaf)	60 °C overnight + calcination 400 °C	Zinc nitrate hexahydrate	20 nm Rods	Antibiofilm and antioxidant potential against food-borne pathogens	(41)
		Pine			
Pinus brutia (leaf)	75 °C for 30 min + 75 °C for 8 h + 2 h calcination at 500 °C calcination	Zinc nitrate hexahydrate	37-74 nm Hexagonal	Dye degradation	(22)
Pinus latteri	90 °C for 90 min + 60 min + calcination 600 °C for 120 min	Zinc chloride	30-100 nm Hexagonal	Photocatalysis and antibacterial	(42)
Pinus densiflora (pinecones)	80 °C for 12 h + evaporation 100–150 °C for 10–12 h+ calcined at 400 °C for 1 h	Zinc nitrate	10-100 nm Hexagonal (wurtzite), triangular,	Antibacterial and antifungal	(43)

			spherical, and oval-shaped		
Pine (leaf)	75 °C for 8h + calcination 550 °C for 3 h	Zinc nitrate	56 nm Nanocomposites	Removal of heavy metals from aqueous media	(44)

A.2 Green Synthesis

The green synthesis method specified in Chapter 2.2 can be summarized in Figure 19.

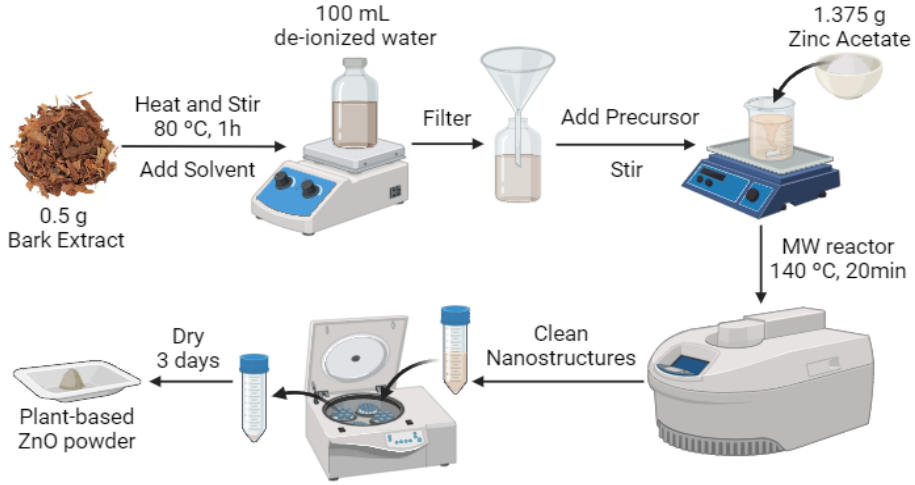

Figure 17. Illustration of the green synthesis of ZnO nanostructures from plant extracts by a solvothermal method assisted with a MW. Created in BioRender.com

A.3 DSC

In Chapter 3.1.1.1 the working temperatures regarding the different plant extracts were retrieved with the data from Figures 20, 21, and 22.

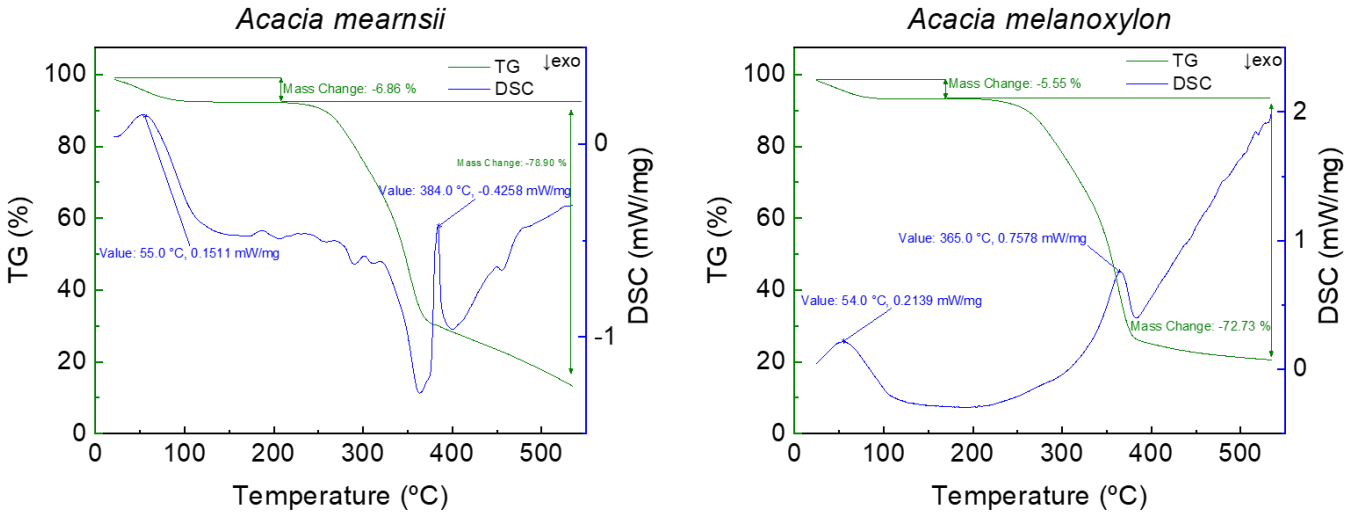

Figure 18. *Acacia mearnsii* and *melanoxylon* simultaneous thermal analysis with DSC.

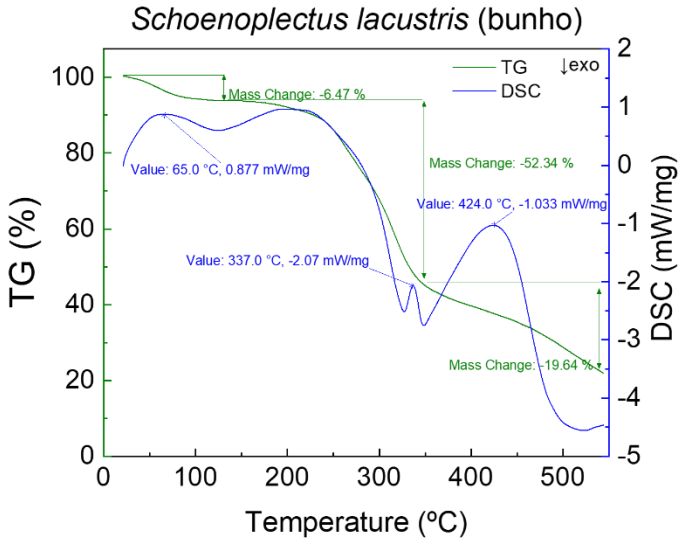

Figure 20. *Schoenoplectus lacustris* (bunho) extracts simultaneous thermal analysis with DSC.

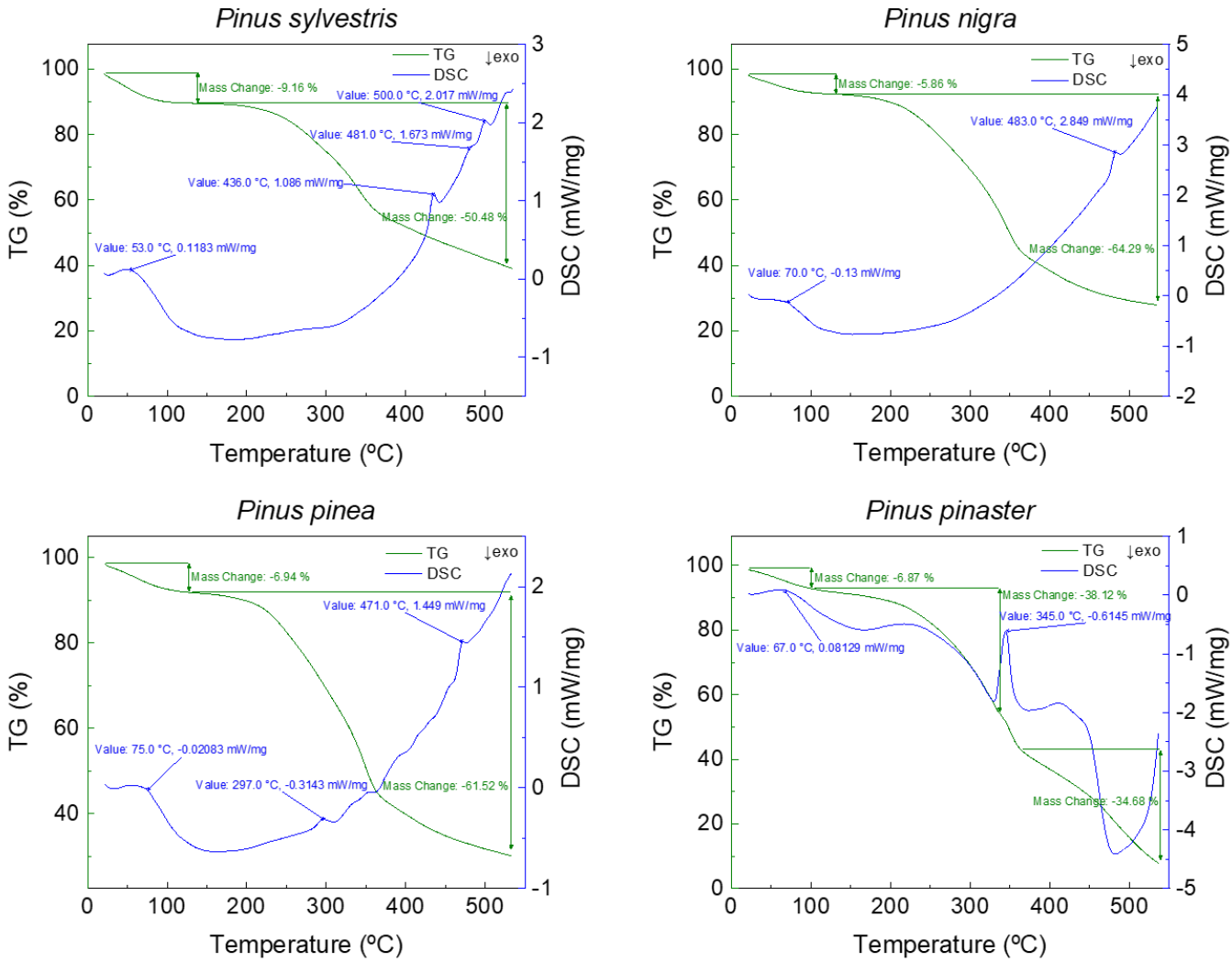

Figure 19. *Pinus sylvestris*, *nigra*, *pinea*, and *pinaster* extracts simultaneous thermal analysis with DSC.